

Experimental Characterization of Micro-Friction on a Mica Surface Using the Lateral Motion and Force Measurement Capability of an Instrumented Indenter

Abhishek Srivastava · Karl J. Astrom ·
Kimberly L. Turner

Received: 10 September 2006 / Accepted: 17 May 2007 / Published online: 6 June 2007
© Springer Science+Business Media, LLC 2007

Abstract An experimental characterization of friction forces between asymmetric surfaces in the micro-regime is presented. The lateral motion and force-measurement capability of an instrumented indenter (triboindenter) is characterized and explored for determining friction properties at low velocities. Friction experiments are performed using the triboindenter with high repeatability. It is observed that real-time depth measurements closely follow the Hertzian prediction. Friction spikes with magnitudes depending on the drive velocity input are observed with peak friction force increasing with the dwell time. Anisotropy is observed between surfaces of different materials with stick-slip occurring only at specific relative orientations. Directions for expanding the current range of the triboindenter to obtain data from the nano to the macro scale are also presented.

Keywords Adhesion · Stiction · Static friction · Stick-slip · Unlubricated friction · Friction test methods · Aluminum · Diamond

Introduction

Over virtually all length scales from nano to macro, friction can have both positive and negative effects, depending on

the application [1–5]. High surface-to-volume ratios among sliding or contacting surfaces over small scales in micro- and nanoelectromechanical (MEMS/NEMS) systems can lead to severe loss of functionality in these devices due to friction. On the other hand, friction drives such as scratch drives utilize friction to enable the motion of free-standing structures using microactuators [6, 7]. Friction-related issues are ubiquitous and many MEMS devices are particularly susceptible to untimely failure caused by friction-induced wear [8–11]. The effects of friction are also relevant in many other application areas, for example, in high-precision positioning where friction can lead to tracking errors, limit cycles and an undesired stick-slip motion. While the effects of friction can cause significant problems in many applications, the fundamental understanding of the friction phenomenon could be substantially increased with improved measurement techniques. For example, in friction-based MEMS devices operating at high frequencies, models for simulating friction behavior at micro-scales require precise experimental data at those scales, while for control applications precise measurements at low-tracking speeds are critical for improving friction compensation [12–14].

An important challenge in the development of friction models has been the lack of accurate friction data and reliable instruments for obtaining essential data. The Atomic Force Microscope (AFM) [15], Surface Force Apparatus (SFA) [6], and the Scanning Force and Friction Microscope (SFFM) [7] have been developed and used in recent years for tribological studies [16]. The AFM and the SFFM are, however, restricted to very low load and very small motions (nearly atomic). Using the lateral motion and force-measurement capability of an instrumented indenter referred to as the triboindenter, we have performed experiments to increase an understanding of friction at the micro-scale.

A. Srivastava (✉) · K. J. Astrom · K. L. Turner
Department of Mechanical and Environmental Engineering,
University of California, Santa Barbara, CA 93106, USA
e-mail: asrivast@engineering.ucsb.edu

K. J. Astrom
e-mail: kja@control.lth.se

K. L. Turner
e-mail: turner@engineering.ucsb.edu

Experimental Setup

Transducer Design and Characterization

The triboindenter is a nanomechanical testing system for characterization of materials on nanometer length scales. It is used to characterize materials by making a small indentation using tips with well-defined geometry. Force and displacement data from the indentation can be used to extract material properties of the sample including the Young's modulus, hardness, viscoelasticity, and fracture toughness [17]. The instrument is also suited for friction experiments because normal and lateral forces can be accurately controlled and measured through feedback. This instrument has previously been used to quantify scratch resistance [Pontin, M., Moses, D., Waite, J., Zok, F.: A Nonmineralized Approach to Abrasion Resistant Biomaterials. Unpublished Work], microwear properties [18], friction coefficients, and depth of wear [19].

The apparatus is shown in Fig. 1. The instrument is mounted on a vibration-isolation platform inside a plastic enclosure. The sample is mounted on the stage, while the optics are located to its right. A three-axis piezo-scanner provides nano scale positioning of the triboindenter tip. The force/displacement transducer consists of a capacitive core having two fixed outer plates and a spring suspended center plate to which the indenter tip is attached [17]. The center plate is actuated electrostatically and the resulting displacement is detected by capacitive sensing. For lateral motion, two additional force-displacement sensors in vertical orientation are provided creating a 2D transducer system. In that case, the x-axis is under displacement control instead of force control.

The velocity and the normal force can be precisely controlled. Friction tests are set up by specifying the normal load and the displacement as functions of time. The maximum velocity is 1 mm/s, but the maximum lateral displacement is limited to about 18 μm . As a result, in our experiments the velocity was limited to 40 $\mu\text{m/s}$ to allow the friction force to develop and achieve steady state. The instrument's lower-velocity resolution threshold was experimentally determined to be 0.1 $\mu\text{m/s}$. The effective

velocity range of the instrument for friction measurements is thus 0.1–40 $\mu\text{m/s}$.

Tilt-Correction

Since, there is no way to accurately determine the sample tilt with respect to the tip, a tilt-correction feature provided by the instrument's vendor was used. Sample tilt is calculated from the initial motion of the tip when no normal force is applied and compensated for. Also, a small-lateral force always appears during the loading period of the stationary tip. Assuming this force is caused because of the tilt in the sample, it should change direction along the measurement axis when the sample is rotated. A mica sample was rotated through 360° and a friction force is not observed to change its direction although its magnitude varied at different rotation angles. This ruled out the possibility of the friction force being caused solely due to tilt in the sample, indicating a tilt in the triboindenter transducer-tip assembly itself. Data from the mica sample rotated through 360° was used to compute the overall tilt angle at different sample orientations, and its mean value was found to be approximately 1.5° with a standard deviation of 0.5° that could be attributed to the existing sample tilt at various locations and orientations. This measured tilt in the triboindenter transducer-assembly could be the result of a misalignment during production or initial system setup and might be limited to the particular instrument used in our experiments. For use in friction measurements it would be highly desirable if the tilt of the transducer-tip assembly could be adjusted prior to experimentation.

Tip Geometry

A cono-spherical tip, as shown in Fig. 2(a), facilitates alignment for friction testing on harder materials when no plastic deformation is desired. By choosing a tip with high radius (50 μm), a relatively flat surface-to-sample contact could be achieved and parallelism issues associated with flat tips can be avoided. Diamond (recently proposed as an alternative material for friction-based MEMS devices [20]) has been used as the tip material. An AFM image of the 50 μm 90° cone angle tip, which is used in most of our

Fig. 1 Photograph of the triboindenter setup showing the various components.

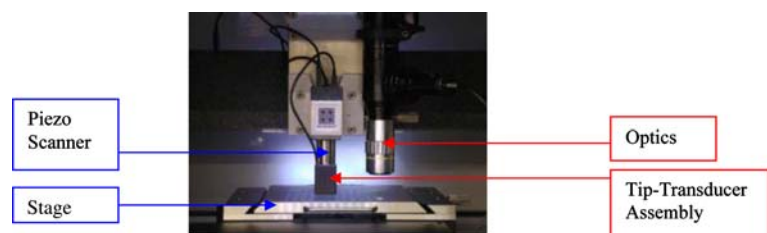
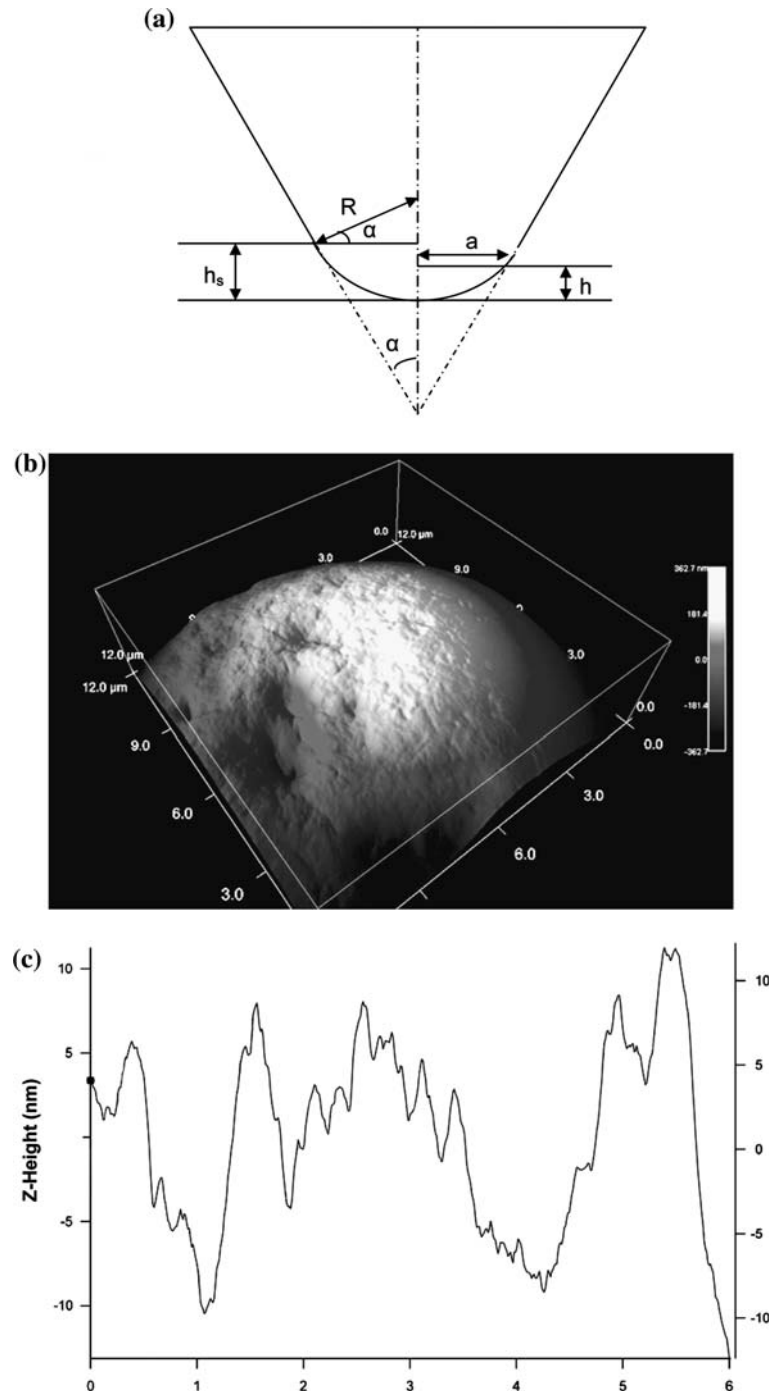


Fig. 2 (a) Geometry of a cono-spherical tip. R = probe radius, α = $\frac{1}{2}$ included angle of probe, h_s = transition depth from spherical to conical, h = contact depth, a = contact radius. (b) AFM image of the 50 μm , 90 deg cono-spherical diamond tip taken using Asylum's MFP-3D system. The surface of the tip is irregular. (c) Trace along a section of the tip.



experiments, is shown in Fig. 2(b). The tip has a number of irregular features which are important in explaining some of the friction results obtained.

Sample Preparation and Characterization

Mica was used as one of the contacting surfaces since it has atomically flat planes. A mica sample was glued to a 15 mm diameter steel plate and cleaved using adhesive tape before being brought into contact with the tip. An

AFM image of the mica sample shows the peak surface height to be about 1.1 Å, which is in good agreement with reported surface heights in the range of 0.91–1.05 Å [21]. The visible asperities are of the order of 10 pm in height and 1 μm in width. The mica surface can thus be considered to be essentially atomically flat. A layer of adsorbed water and organics (~ 2 nm) cannot be completely avoided [22], because all experiments are conducted on dry mica surfaces under atmospheric conditions.

Results and Discussion

Unidirectional friction tests were performed using the triboindenter starting with the calibration of the instrument. Measurements of friction were performed with normal loads in the range of 1–10,000 μN and velocity range of 0.1–40 $\mu\text{m/s}$.

Friction Force vs Normal Load

The friction force obtained using a 50 μm diamond tip sliding on a freshly cleaved mica surface is plotted against the applied normal load measured at a constant velocity of 13.5 $\mu\text{m/s}$. A linear dependence is observed, as shown in Fig. 3 which is in agreement with the Amontons' law of friction, $F = \mu N$ [23] and is similar to the results reported for measurements at this scale [24, 25]. A linear fit gives a friction coefficient, μ , of 0.1, which is slightly lower than the data in [26].

Variation of Friction Force with Velocity

Figure 4 shows the variation of friction force as a function of velocity. For all velocities, the friction data was collected over a fixed range of displacement of 16 μm and the average value was computed. At low normal loads, we see a mostly linear behavior with a slight increase in the friction force as the velocity increases in addition to some non-linearity at low velocities. One possible explanation for this based on reduced time of thermal activation of unstable atoms is given in [27]. This observation is consistent with previous results [24, 28, 29], where it was observed that the friction force increases slightly at low velocities and then settles at constant value for higher velocities. The highest velocity in our measurements was too low to reach steady state.

To test the repeatability of the experiments, the 3000 μN normal load, 13.5 $\mu\text{m/s}$ velocity experiment was executed

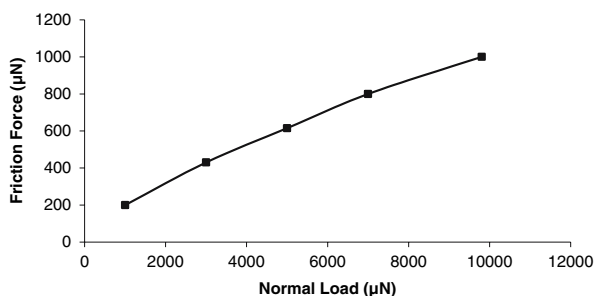


Fig. 3 Friction force vs normal load at a constant velocity of 13.5 $\mu\text{m/s}$. The contacting surfaces are mica and a cono-spherical diamond tip of radius 50 μm . A linear fit gives a friction coefficient of 0.1.

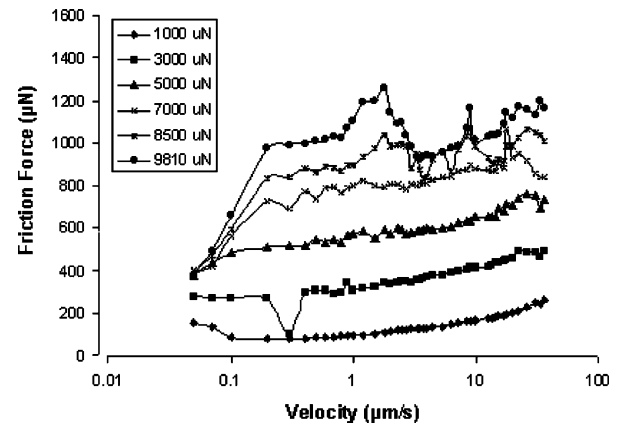


Fig. 4 Friction force as a function of velocity at different normal loads. The contacting surfaces are mica and a cono-spherical diamond tip of radius 50 μm .

five times. The mean friction force was 362.2 μN with a standard deviation of 4.7 μN (1.3%). The average recorded on a different day was 373.9 μN making the standard deviation between the average values of these two days as 8.3 μN (2.2%) which suggests high repeatability of the data obtained from the triboindenter.

Friction traces changed with time and as reported in [30] it took multiple repetitions for the friction traces to reach steady-state conditions. At higher normal loads the steady state was reached in fewer repetitions. For a normal load of 500 μN , it took about six repetitions but only three repetitions were required for a normal load of 5000 μN .

Typical Friction Force Profiles

Typical friction traces observed in measurements with the triboindenter are shown in Fig. 5. For an applied constant velocity, the friction force typically reaches an initial peak and then drops. It then rises again and fluctuates

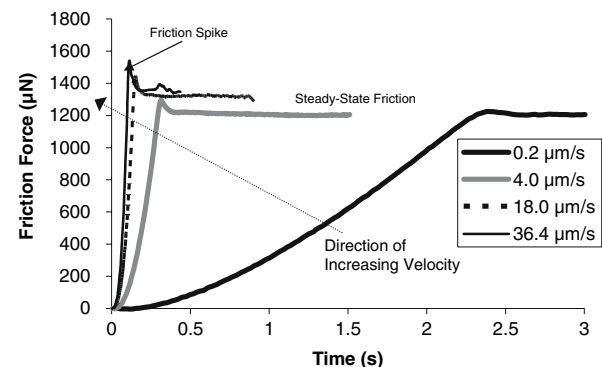
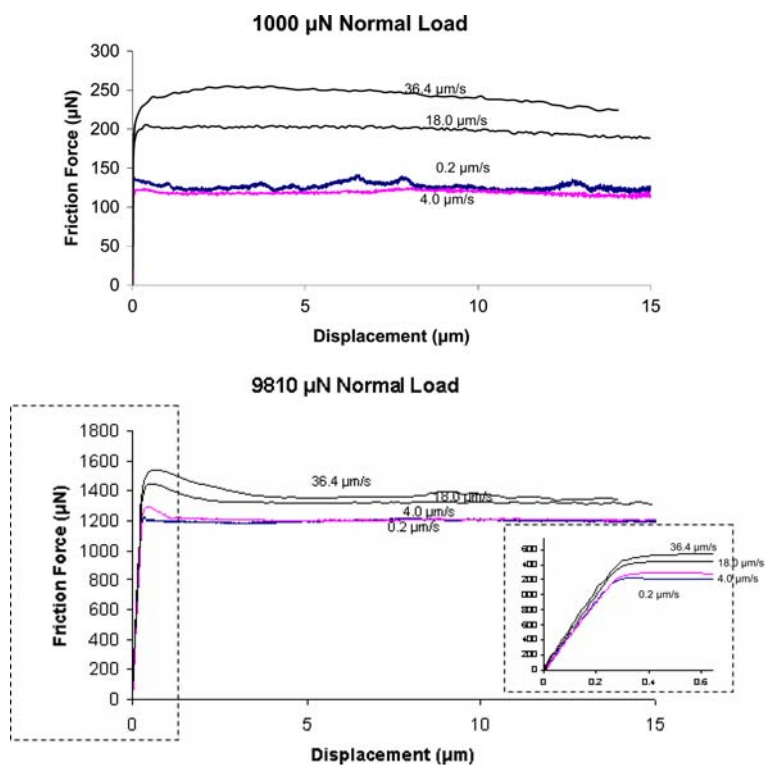


Fig. 5 Time behavior of friction at the start of sliding motion. The contact surfaces are mica and a cono-spherical diamond tip of radius 50 μm . Notice the peak in friction.

Fig. 6 Friction force as a function of displacement for the experiment in Fig. 5 at (a) 1000 μN normal load (b) 9810 μN normal load. The dotted box shows the curves zoomed in at onset of sliding.



around a steady-state value. This phenomenon, observed at the commencement of sliding for two surfaces at rest in adhesive contact is called ‘stiction spike’ [31]. As shown in Fig. 5, the magnitude of the spike increases with increasing velocity. The time taken to reach the peak of the stiction spike decreases with increasing velocity. The results of Fig. 5 have been replotted in Fig. 6 as friction force versus displacement. These curves show spring-like behavior for small displacements with lateral stiffness of about 5000 N/m. The effective stiffness depends on the stiffnesses of the indenter, the control system and the mica-diamond contact. The contact stiffness depends on

the area of contact [32] and a change in the contact area with velocity may explain the observed variation in the lateral stiffness. As seen in Fig. 6(a), velocity weakening [33] occurs for lower normal loads at low velocities. The displacement during this rise time is roughly independent of velocity as reported in [2, 33] but increases with normal load. At higher normal loads, it takes longer time to reach the peak. As shown in Fig. 7, the peak friction force increases with dwell time. One hypothesis is that the binding force between the two surfaces increases with the contact time leading to an overall increase in the friction force.

Depth Measurements and their Variation with the Tip Geometry

The triboindenter gives real-time depth measurements during the friction tests. When the lateral motion starts, the maximum depth first reaches a peak value and then typically fluctuates around that value until the tip is withdrawn from the sample. Figure 8 shows a plot of the maximum depth at various normal loads for the entire velocity range. This curve closely follows the Hertzian prediction, thus suggesting that the deformation during the lateral motion is purely elastic.

Testing with softer materials such as aluminum, increased friction force is observed for the 5 μm tip over the 50 μm tip, other factors remaining the same. As

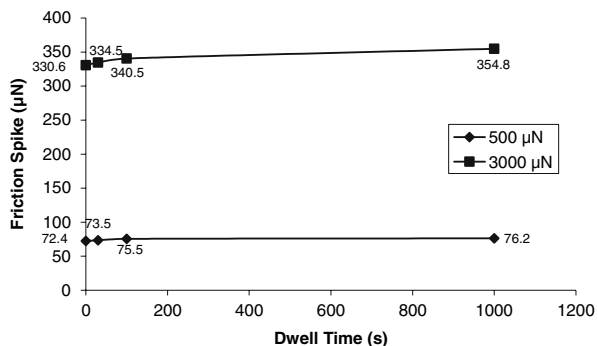


Fig. 7 Effect of resting time after load application on peak value of friction spike. The contacting surfaces are mica and a cono-spherical diamond tip of radius 50 μm .

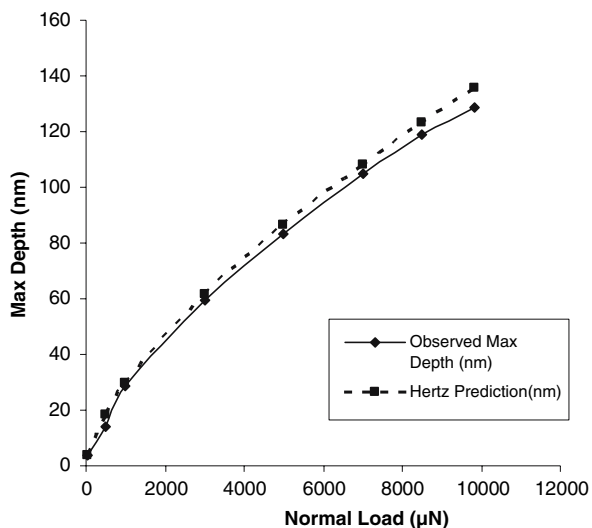


Fig. 8 Maximum depth versus applied normal load and comparison with Hertz prediction for given tip geometry. The contacting surfaces are mica and a conospherical diamond tip of radius 50 μm .

shown in Fig. 9, this effect is opposite to that observed in case of mica. The softness of the aluminum sample could possibly lead to more penetration by the sharper 5 μm tip, thus producing a higher friction force than that

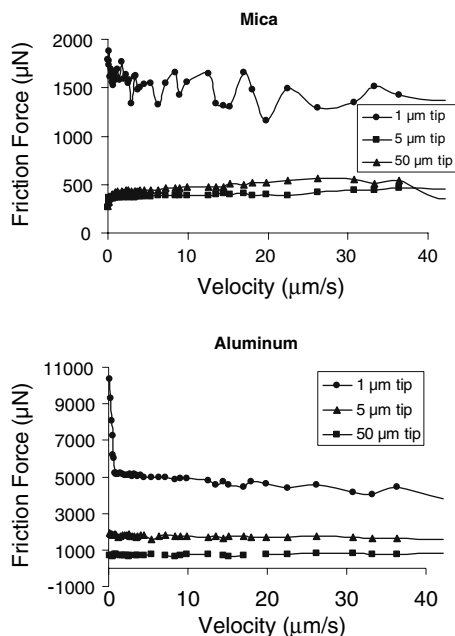


Fig. 9 Friction force as a function of velocity for 5000 μN normal load for diamond tips with radii 1 μm , 5 μm and 50 μm diamond tips for (a) mica surface and (b) aluminum surface. In case of mica, the friction force measured with the 5 μm tip is lower than that observed with the 50 μm tip whereas the opposite trend is observed in case of aluminum.

produced by the 50 μm tip therefore giving results which are more suggestive of fracture than friction. On the other hand, being harder, mica does not allow for such deep penetration of the 5 μm tip and the contact area is much smaller, closely following Hertz prediction. In both cases, similar friction experiments conducted with the 1 μm cono-spherical tip yield much higher values for friction forces than that obtained by the 5 μm tip or the 50 μm tip. Depth measurements show that the sharper 1 μm tip penetrates further into both the samples and in the case of aluminum it even fails to yield meaningful friction data in cases where the tip gets stuck in the soft sample. A typical lateral force profile produced by the 1 μm tip in mica is shown in Fig. 10(a) indicating that the tip moves across various points in the direction of motion in a stop-jump fashion, penetrating deep into the surface at each contact. For experiments with the 50 μm tip, surface damage due to tip indentation are visually observed under a microscope for normal loads 250 mN and higher.

Stick-Slip and Anisotropy

Stick-slip, as shown in Fig. 10(b), was a rare occurrence in experiments with the 50 μm tip sliding against a mica surface and it also exhibited dependence on the relative orientations of the two samples. Fig. 11 shows the variation of the average friction force with respect to the sample rotation and stick-slip is observed at angles that give the highest friction. In [34], the frictional anisotropy between mica–mica interface has been attributed to the commensurability between the contacting lattices, whereas in [35], the authors state that when the surfaces deform plastically under shear, friction anisotropy originates with the properties of the bulk crystal lattices. In our case the materials in contact are different in nature and neither of the above explanation applies directly. Apart from the difference in material, one possible reason for this irregularity could be that the circular radius of Hertzian contact between the 50 μm diamond conospherical tip and the mica surface (parameter a in Fig. 1) is limited to 2 μm . Also, the irregularity in the geometry of the 50 μm diamond tip shown in Fig. 2 could cause fewer contact points between the tip and the sample, leading to non-uniformity in the nature of stick-slip. The magnitude of stick-slip decreases with increasing velocity similar to what has been reported in [36]. No significant variation in friction force due to anisotropy was observed in similar tests with single-crystal silicon with a cubically symmetric lattice structure, indicating that the crystal structure of the substrate rather than that of the diamond tip might be the determining factor for the occurrence of anisotropy.

Fig. 10 (a) Friction force as a function of time for a 1 μm diamond tip on mica. The applied normal load is 5000 μN and the velocity is 0.2 $\mu\text{m/s}$. (b) Typical stick-slip results for a mica substrate using 50 μm cono-spherical diamond tip under an applied normal load of 9810 μN and velocity 1.5 $\mu\text{m/s}$.

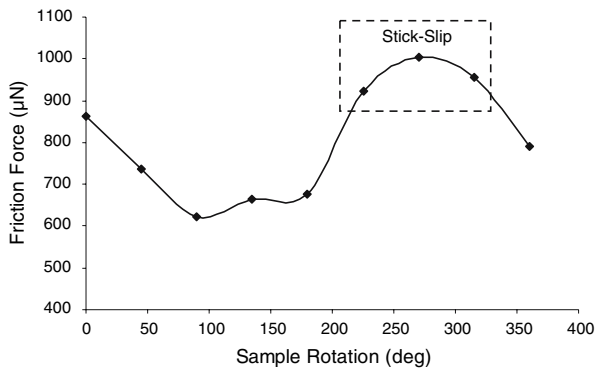
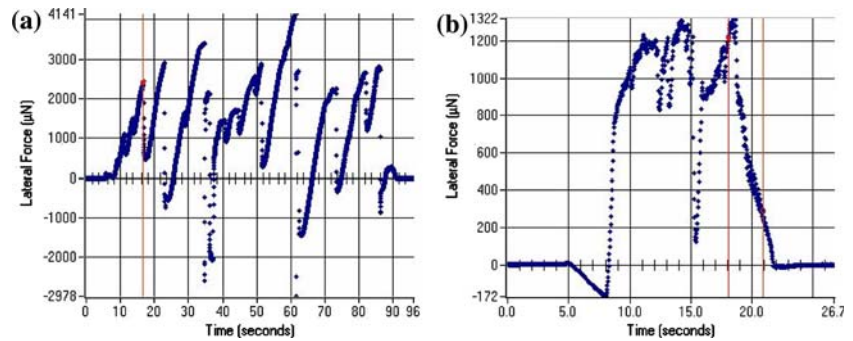


Fig. 11 Anisotropy in friction for mica substrate and a 50 μm cono-spherical diamond tip. Stick-slip is observed at orientations at which the measured friction force is the highest. The applied normal load is 9810 μN and the velocity is 1.5 $\mu\text{m/s}$. The mica sample is rotated successively by 45° between measurements.

Conclusion

The triboindenter has been explored as a device for performing friction experiments at the micro-scale for small displacements and low velocities. The results are highly repeatable and it is important that a tip with large radius is used. Friction spikes achieve higher peaks in reduced rise times as the velocity is increased. Anisotropy is observed between asymmetric surfaces with stick-slip occurring only at specific relative orientations. Depth measurements correspond to values predicted by Hertzian contact theory. The maximum normal load of the instrument is 10 mN and the displacement range is limited to 18 μm . The authors are currently exploring new extensions to the current setups, which allow normal loads up to 5 N and a velocity range of 4 \AA/s –1 mm/s. Such an extended measurement range could help bridge the gap of measurements between the atomic and macro scales.

Acknowledgments We are very grateful to Jacob Israelachvili and Kenny Rosenberg for sharing their deep insight into friction and its measurements. Seth Downs and Richard Nay at Hysitron Inc. assisted us in using the triboindenter and advanced instrumentation, and in interpreting the results. Alejandro Bonilla at Asylum helped us obtain

the AFM images of the tip on their MFP3D system. This work was supported in part by NSF Award # 0414298.

References

- Dowson, D.: History of Tribology. Longman Group United Kingdom, London (1979)
- Armstrong-Helouvry, B.: Control of Machines with Friction. Kluwer Academic Publishers (1991)
- Dieterich, J.: Modeling of rock friction 1. Experimental results and constitutive equations. *J. Geophys. Res.* **84**, 2161–2168 (1979)
- Pacejka, H.: Tyre and Vehicle Dynamics. Butterworth-Heinemann (2002)
- Bhushan, B.: Handbook of Micro/Nano Tribology, 2nd edn. CRC Press LLC (1999)
- Akiyama, T., Shono, K.: Controlled stepwise motion in polysilicon microstructures. *J. Microelectromech. Syst.* **2**, 105–110 (1993)
- deBoer, M., Luck, L., Ashurst, W., Maboudian, R., Corwin, A., Walraven, J., Redmond, J.: High-performance surface micromachined inchworm actuator. *J. Microelectromech. Syst.* **13**, 63–74 (2004)
- Tanner, D., Walraven, J., Mani, S., Swanson, S.: Pin-joint design effect on the reliability of a polysilicon microengine. In: Proceedings of IRPS (2002)
- Subhash, G., Corwin, A., deBoer, M.: Operational wear and friction in MEMS devices. In: Proceedings of IMECE04, CA (2004)
- Davies, R., Rodgers, M., Montague, S.: Design tools and issues of silicon micromachined (MEMS) devices. In: 2nd International Conference on Engineering Design and Automation, Maui, Hawaii (1998)
- Miller, S., Sniegowski, J., LaVigne, G., McWhorter, P.: Friction in surface micromachined microengines. In: Proceedings of SPIE Smart Electronics and MEMS, San Diego, CA (1996)
- Wit, C., Aström, K., Braun, K.: Adaptive friction compensation in DC motor drives. *IEEE J. Robot. Autom.* **3**, 681–685 (1987)
- Wit, C., Olsson, H., Aström, K., Lischinsky, P.: A new model for control of systems with friction. *IEEE T. Automat. Control* **40**, 419–425 (1995)
- Olsson, H., Aström, K.: Friction Generated Limit Cycles. *IEEE T. Control Syst. Technol.* **9**, 629–636 (2001)
- Binnig, G., Quate, C., Gerber, C.: Atomic force microscope. *Phys. Rev. Lett.* **56**, 930–933 (1986)
- Gao, J., Luedtke, W., Gourdon, D., Ruths, M., Israelachvili, J., Landman, U.: Frictional forces and Amontons' law: from the

- molecular to the macroscopic scale. *J. Phys. Chem. B.* **108**, 3410–3425 (2004)
17. Hysitron, Inc.: *Tribointender Users Manual*: Hysitron Incorporated 5251 West 73rd Street, Minneapolis, MN 55439 (2001)
 18. Rohde, S., Mihut, D., Aouadi, S., Turner, J.: Nanotribological properties of nanocomposite CrBN and TiBN thin films. In: *Proceedings of 3rd International Surface Engineering Congress*, Orlando, FL (2004)
 19. Schiffmann, K., Hieke, A.: Analysis of microwear experiments on thin DLC coatings: friction, wear and plastic deformation. *Wear* **254**, 565–572 (2003)
 20. Sumant, A., Grierson, D., Gerbi, E., Birrell, J., Lanke, U., Auciello, O., Carlisle, J., Carpick, R.: Toward the ultimate tribological interface: surface chemistry and nanotribology of ultrananocrystalline diamond. *Adv. Mater.* **17**, 1039–1045 (2005)
 21. Nambda, Y., Yu, J., Bennett, J., Yamashita, K.: Modeling and measurements of atomic surface roughness. *Appl. Optics* **39**, 2705–2718 (2000)
 22. Israelachvili, J., Alcantar, N., Maeda, N., Mates, T., Ruths, M.: Preparing contamination-free mica substrates for surface characterization, force measurements, and imaging. *Langmuir* **20**, 3616–3622 (2004)
 23. Amontons, G.: De la resistance caus'ee dans les machines. *Memoires de l'Academie Royale A*, 257–282 (1699)
 24. Tocha, E., Stefanski, T., Schönherr, H., Vansco, G.: Development of a high velocity accessory for atomic force microscopy-based friction measurements. *Rev. Sci. Inst.* **76**, 083704–083707 (2005)
 25. McGuiggan, P., Zhang, J., Hsu, S.: Comparison of friction measurements using the atomic force microscope and the surface forces apparatus: the issue of scale. *Tribol. Lett.* **10**, 217–223 (2001)
 26. Tang, H., Joachim, C., Devillers, J.: Interpretation of atomic force microscopy images: The mica (001) surface with a diamond tip apex. *J. Vac. Sci. Tech. B: Microelectron. Nanometer Struct.* **12**, 2179–2183 (1994)
 27. He, G., Robbins, M.: Simulations of the kinetic friction due to adsorbed surface layers. *Tribol. Lett.* **10**, 7–14 (2001)
 28. Gnecco, E., Bennewitz, R., Gyalog, T., Loppacher, C., Bammerlin, M., Meyer, E., Güntherodt, H.: Velocity dependence of atomic friction. *Phys Rev. Lett.* **84**, 1172–1175 (2000)
 29. Ohnishi, S., Stewart, A.: Humidity dependence of interfacial friction between mica surfaces. *Langmuir* **18**, 6140–6146 (2002)
 30. Gourdon, D., Israelachvili, J.: Transitions between smooth and complex stick-slip sliding of surfaces. *Phys. Rev. E* **68**, 021602-1–021602-10 (2003)
 31. Maeda, N., Chen, N., Tirrell, M., Israelachvili, J.: Adhesion and friction mechanisms of polymer-on-polymer surfaces. *Science* **297**, 379–382 (2002)
 32. Carpick, R., Ogletree, D., Salmeron, M.: Lateral stiffness: a new nanomechanical measurement for the determination of shear strengths with friction force microscopy. *Appl. Phys. Lett.* **70**, 1548–1550 (1997)
 33. Baumberger, T., Berthoud, P., Caroli, C.: Physical analysis of the state- and rate-dependent friction law. II. Dynamic friction. *Phys. Rev. B.* **60**, 3928–3939 (1999)
 34. Hirano, K., Kaneko, R., Murata, Y.: Anisotropy of frictional forces in muscovite mica. *Phys. Rev. Lett.* **67**, 2642–2645 (1991)
 35. Mancinelli, C., Gellman, A.: Friction Anisotropy at Pd(100)/Pd(100) Interfaces. *Langmuir* **20**, 1680–1687 (2004)
 36. Israelachvili, J., Berman, A.: Surface Forces and Microrheology of Molecularly Thin Liquid Films. *Handbook of Micro/Nano Tribology*, pp. 371–432 (1999)